

GENERAL ARTICLE

Pmp22 super-enhancer deletion causes tomacula formation and conduction block in peripheral nerves

Harrison Pantera^{1,2,†}, Bo Hu^{5,†}, Daniel Moiseev⁵, Chris Dunham⁵, Jibraan Rashid⁵, John J. Moran¹, Kathleen Krentz⁴, C. Dustin Rubinstein⁴, Seongsik Won¹, Jun Li⁵ and John Svaren^{1,3,*,‡}

¹Waisman Center, University of Wisconsin-Madison, Madison, WI 53705, USA, ²Molecular and Cellular Pharmacology Graduate Program, University of Wisconsin-Madison, Madison, WI 53705, USA, ³Department of Comparative Biosciences, University of Wisconsin-Madison, Madison, WI 53705, USA, ⁴Biotechnology Center, University of Wisconsin-Madison, Madison, WI 53705, USA and ⁵Department of Neurology and Translational Neuroscience Initiative, Wayne State University School of Medicine, Detroit, MI 48202, USA

*To whom correspondence should be addressed at: Waisman Center, University of Wisconsin-Madison, 1500 Highland Ave, Madison, WI 53705, USA. Tel: 608 2634246; Email: john.svaren@wisc.edu

Abstract

Copy number variation of the peripheral nerve myelin gene *Peripheral Myelin Protein 22* (*PMP22*) causes multiple forms of inherited peripheral neuropathy. The duplication of a 1.4 Mb segment surrounding this gene in chromosome 17p12 (c17p12) causes the most common form of Charcot-Marie-Tooth disease type 1A, whereas the reciprocal deletion of this gene causes a separate neuropathy termed hereditary neuropathy with liability to pressure palsies (HNPP). *PMP22* is robustly induced in Schwann cells in early postnatal development, and several transcription factors and their cognate regulatory elements have been implicated in coordinating the gene's proper expression. We previously found that a distal super-enhancer domain was important for *Pmp22* expression *in vitro*, with particular impact on a Schwann cell-specific alternative promoter. Here, we investigate the consequences of deleting this super-enhancer *in vivo*. We find that loss of the super-enhancer in mice reduces *Pmp22* expression throughout development and into adulthood, with greater impact on the Schwann cell-specific promoter. Additionally, these mice display tomacula formed by excessive myelin folding, a pathological hallmark of HNPP, as have been previously observed in heterozygous *Pmp22* mice as well as sural biopsies from patients with HNPP. Our findings demonstrate a mechanism by which smaller copy number variations, not including the *Pmp22* gene, are sufficient to reduce gene expression and phenocopy a peripheral neuropathy caused by the HNPP-associated deletion encompassing *PMP22*.

Introduction

Proper myelination by Schwann cells in the peripheral nervous system depends in part on coordinated expression of key structural myelin proteins (1). One of these proteins is encoded by the *peripheral myelin protein 22* (*PMP22*) gene, which is included in a

1.4 Mb duplication that causes the most common form of inherited peripheral neuropathy, called Charcot-Marie-Tooth disease type 1A (CMT1A) (2–5). This progressive sensorimotor polyneuropathy is marked by dysmyelination with shortened internodes (6–9), ultimately leading to degeneration of the myelin and

[†]The authors wish it to be known that, in their opinion, the first 2 authors should be regarded as joint first authors.

[‡]John Svaren, <http://orcid.org/0000-0003-2963-7921>

Received: February 28, 2020. Revised: April 7, 2020. Accepted: April 24, 2020

© The Author(s) 2020. Published by Oxford University Press. All rights reserved. For Permissions, please email: journals.permissions@oup.com

axons, and weakness and atrophy in those denervated limb muscles. The reciprocal 1.4 Mb deletion, resulting in inheritance of only one copy of the *PMP22* gene, causes a distinct neuropathy known as hereditary neuropathy with liability to pressure palsies (HNPP) (10–14). HNPP is pathologically characterized by paranodal hypermyelination, causing tomacula formation. The disease commonly manifests as focal sensory loss and muscle weakness when the affected nerves are exposed to mild mechanical compression innocuous to healthy people but resulting in conduction block (failure of action potential propagation) in HNPP patients. Though less severe phenotypically, HNPP may cause severe limb paralysis when asymptomatic patients with unknown diagnosis of HNPP are challenged by strenuous physical activities (15). This imposes a catastrophic risk in a fraction of patients with HNPP.

Given that *PMP22* gene dosage variation in either direction may cause peripheral neuropathy, it is of interest to understand endogenous mechanisms that regulate the gene's expression, which could have therapeutic implications (16). *PMP22* encodes one of the most abundantly expressed transcripts in mature peripheral nerve in RNA-seq studies (17). Two major promoters P1 and P2 drive the expression of *PMP22* using two alternate non-coding exons (1A or 1B, respectively) and the relative abundance of these alternative transcripts is approximately 3:1 in rodents (18) and 1:1 in human Schwann cells (as recently confirmed in gtexportal.org). The P1 promoter is expressed exclusively in myelinating Schwann cells, although both P1 and P2 transcripts are induced during myelination. In other tissues where *PMP22* is expressed at a lower level, the P2 transcript is the major form. Transgenic analysis identified an enhancer region upstream of the P1 promoter (19, 20), known as the late myelination Schwann cell-specific element (LMSE). However, neither the promoters nor the LMSE could recapitulate the large developmental induction of *Pmp22* in transgenic assays.

Using ChIP-seq analysis, we had identified a ~40 kb super-enhancer domain termed *Pmp22*-SE upstream of the rat *Pmp22* gene (21, 22). This domain falls within a larger 168 kb region in overlapping upstream duplications (not including the *PMP22* gene) identified in patients presenting with mild CMT-like symptoms (23, 24). The enhancers are largely absent from oligodendrocytes where *PMP22* is expressed at a much lower level (4, 18, 21), and enhancer marks are significantly diminished after nerve injury when the expression of *Pmp22* declines precipitously (25, 26). Using clustered regularly interspaced short palindromic repeats/CRISPR associated protein 9 (CRISPR/Cas9), we deleted this super-enhancer in the S16 rat Schwann cell line and found that the loss of this super-enhancer significantly reduced *Pmp22* transcription, with stronger impact on transcription from the Schwann cell-specific P1 promoter (27).

Since its discovery as a causative agent in inherited neuropathies, several studies have probed the molecular function of *PMP22* using rodent models possessing *Pmp22* deletion (28–35). This led to the discovery that conduction block occurs in these models well before the appearance of segmental demyelination (stripping myelin off the axon) (30). This early 'functional demyelination' (31) was traced to a disruption of myelin junction protein complexes by hyperactive p21-activated kinase (PAK1)-driven actin polymerization in the absence of sufficient levels of *PMP22* protein (33). Interestingly, the elevated activation of PAK1 observed in *Pmp22*^{+/-} mice is further increased following ablation of $\beta 4$ integrin (34), a laminin receptor subunit linked to myelin stability (36, 37). The improper formation of these junction complexes prevents sealing of the myelin sheath, increasing myelin permeability and therefore reducing its capacitance to

function as an insulator (31). In the present study, we explore the presentation of this HNPP phenotype at different levels of *Pmp22* expression in mice possessing heterozygous and homozygous loss of the upstream super-enhancer.

Results

Effects of *Pmp22*-SE deletion on *Pmp22* expression

To assess the physiological relevance of the *Pmp22* super-enhancer *in vivo*, we used CRISPR-Cas9 to create a 40.5 kb deletion encompassing the super-enhancer domain in C57BL/6 mice (Fig. 1). The figure depicts the position of the super-enhancer relative to ChIP-seq analysis of the active enhancer mark, histone H3K27 acetylation, and the binding sites for EGR2, SOX10 and TAZ transcription factors that have been shown to regulate *PMP22* expression (21, 22, 38–40). The shaded super-enhancer region contains injury-sensitive enhancers that are specifically identified in Schwann cells but not oligodendrocytes (21, 22). There are several genes in the vicinity of these enhancers, but the active ones are shown by ChIP-seq analysis of the active promoter mark, histone H3K4 trimethylation (41). The bottom line depicts the approximate homologous endpoints for the minimal region of overlap of the neuropathy-associated duplications identified upstream of human *PMP22* (23, 24). Most of the intergenic regions are not conserved, but there are high levels of conservation between rat, mouse and human genomes within the previously defined enhancers (21, 22).

Upon identification of the desired deletion, litters were generated containing heterozygous and homozygous deletion of the *Pmp22* super-enhancer along with wild-type littermates. We collected the sciatic nerves from mice at postnatal Days 0, 10 and 56 (P0, P10 and P56 respectively). The P0 time point precedes the period of active myelination and *PMP22* levels along with myelin genes are relatively low in contrast to their peak during active myelination P10–P20. As myelination completes within a few weeks after birth, *PMP22* levels and myelin genes decline somewhat but still remain at high levels in mature nerve (42).

At the perinatal time point (P0), we observed no significant change in total *Pmp22* messenger RNA (mRNA) in either *Pmp22*-SE^{+/-} or *Pmp22*-SE^{-/-} mice relative to wild-type littermates (Fig. 2A). However, when *Pmp22* becomes highly induced at both P10 and P56, we found significant reduction in total *Pmp22* mRNA in both *Pmp22*-SE^{+/-} mice (relative to wild-type littermates) and *Pmp22*-SE^{-/-} mice (relative to both wild-type and *Pmp22*-SE^{+/-} littermates) (Fig. 2B and C). To evaluate the possibility that this decrease in *Pmp22* expression could be attributable to changes in transcription factors regulating *Pmp22*, we also measured expression of other myelin genes, which are controlled by many of the same transcription factors (16, 21, 22, 43–46). We found no changes in either *Mag* or *Mpz* expression at any time point. Finally, we measured expression of the *Tvp23b* transcript, the next closest expressed gene to the super-enhancer. We found a slight but significant increase in *Tvp23b* mRNA at P0, although this effect disappeared by P10, indicating that the super-enhancer's activity is primarily focused on *Pmp22*. The nearby *Tekt3* gene is inactive in Schwann cells (21, 22). In addition to levels of *Pmp22* transcript, we also assessed *PMP22* protein levels by western blot (Fig. 2D) and observed a commensurate decrease in those levels.

Because our *in vitro* model had demonstrated a more pronounced effect of enhancer deletion on the Schwann cell-specific P1 promoter in contrast to the P2 promoter (27), we measured relative expression of transcripts from the P1 and P2

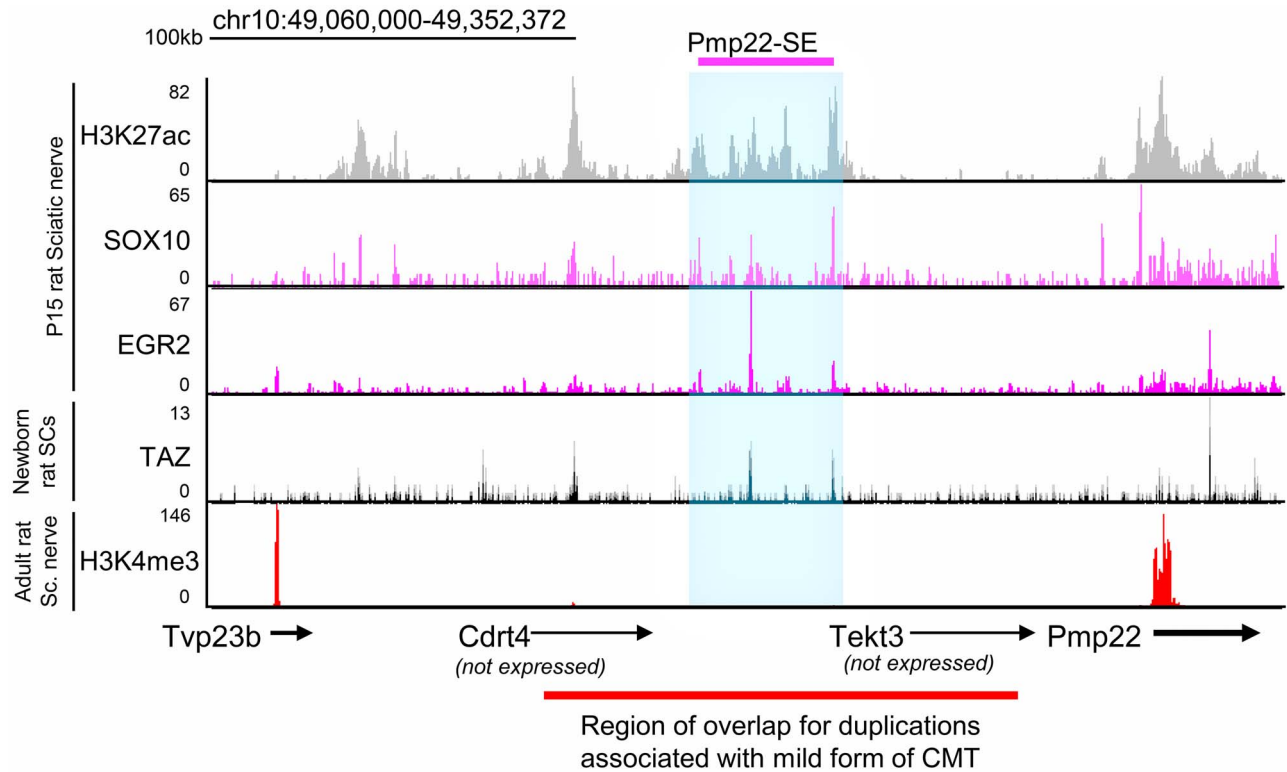


Figure 1. Deletion of *Pmp22*-SE in mice. ChIP-seq analysis in rat peripheral nerve highlights homologous rat sequence deleted in C57/BL6 mice (blue shaded region, corresponding to mm10 chr11:63, 001, 867-63, 042, 405). The super-enhancer region is marked by H3K27ac and contains binding sites for transcription factors SOX10 and EGR2. The absence of H3K4me3, a histone mark associated with active promoters, indicates that *Pmp22*-SE-proximal genes *Cdr4* and *Tekt3* are not expressed in peripheral nerve.

promoters in nerve at these same ages (Fig. 2A–C). At P0, we found a significant decrease in the P1 transcript exclusively in *Pmp22*-SE^{-/-} mice. At P10 and P56, the P1 transcript was significantly reduced in both *Pmp22*-SE^{+/-} mice (relative to wild-type littermates) and *Pmp22*-SE^{-/-} mice (relative to both wild-type and *Pmp22*-SE^{+/-} littermates). Conversely, although the P2 transcript appeared slightly reduced in P0 nerve, we only observed significant reduction of this transcript in P10 nerve from *Pmp22*-SE^{-/-} mice. At P56, the P2 transcript was significantly reduced in both *Pmp22*-SE^{+/-} and *Pmp22*-SE^{-/-} mice. As the P2 transcript is the predominant *Pmp22* transcript in the early postnatal period (18), these results are consistent with our finding that total *Pmp22* is not significantly lower in *Pmp22*-SE^{+/-} or *Pmp22*-SE^{-/-} mice at P0. Therefore, the super-enhancer does not affect *Pmp22* expression in premyelinating Schwann cells. Accordingly, some of the transcription factors that bind to the super-enhancer (such as EGR2) (21, 22) do not become fully induced until later time points (47–49).

We also evaluated additional genes linked to changes in *Pmp22* expression in nerve from P56 *Pmp22*-SE^{+/-} and *Pmp22*-SE^{-/-} mice (Fig. 2D). Consistent with prior reports showing PAK1 mice protein levels are unchanged in heterozygous *Pmp22* deletion mice (33), we detected no significant change in PAK1 mRNA. *Plekha1*, which was reduced by antisense oligonucleotide therapy targeting the *Pmp22* transcript in a rodent model of CMT1A (50), was similarly not affected by deletion of the super-enhancer. We examined *Sipa12* expression because this was recently identified as a modifier gene for CMT1A. *Sipa12* expression is SOX10-regulated and positively correlated with *Pmp22* expression (51) and was slightly but significantly reduced in *Pmp22*-SE^{-/-} mice.

Socs3 and *Id2*, which were previously found to be upregulated in *Pmp22* knockout mice (52), are both significantly elevated in nerve from P56 super-enhancer deletion mice, with *Socs3* transcripts increased in both *Pmp22*-SE^{+/-} and *Pmp22*-SE^{-/-} mice and *Id2* transcripts increased in *Pmp22*-SE^{-/-} mice. Finally, *ApoE* and *Abca1*, genes related to cholesterol efflux, are both elevated in *Pmp22*-SE^{-/-} mice at P56, in line with a recent study of *Pmp22* KO mice (35).

Tomacula formation and aberrant F-actin polymerization in *Pmp22*-SE^{+/-} and *Pmp22*-SE^{-/-} nerve

Previous studies of rodent models of heterozygous *Pmp22* deletion (12, 13, 29, 33, 34) showed tomacula formation and aberrant F-actin polymerization. Similarly, there are myelin structural abnormalities in nerve from adult *Pmp22*-SE^{+/-} and *Pmp22*-SE^{-/-} nerve (Fig. 4A). In teased nerve fibers, increased tomacula in both *Pmp22*-SE^{+/-} and *Pmp22*-SE^{-/-} mice are evident relative to wild-type littermates (Fig. 3A and B). Consistent with the elevated actin polymerization in heterozygous *Pmp22* knockout mice (33), F-actin was elevated at mesaxons (Fig. 3C). We also measured F-actin levels in Schmidt-Lanterman incisures. Again, it was increased in both heterozygous and homozygous *Pmp22*-SE deletion mice (fluorescence intensity: *Pmp22*-SE^{+/+} 630.5 ± 71.9 versus *Pmp22*-SE^{+/-} 958.0 ± 88.1 or *Pmp22*-SE^{-/-} 1105.7 ± 225.0; 80–100 fibers per mouse; n = 3 mice per genotypic group; P < 0.05). Notably, with respect to tomaculus prevalence, the proportion of F-actin positive mesaxons and F-actin fluorescence intensity in incisures, there were no significant differences between *Pmp22*-SE^{+/-} and *Pmp22*-SE^{-/-} mice (Fig. 3D).

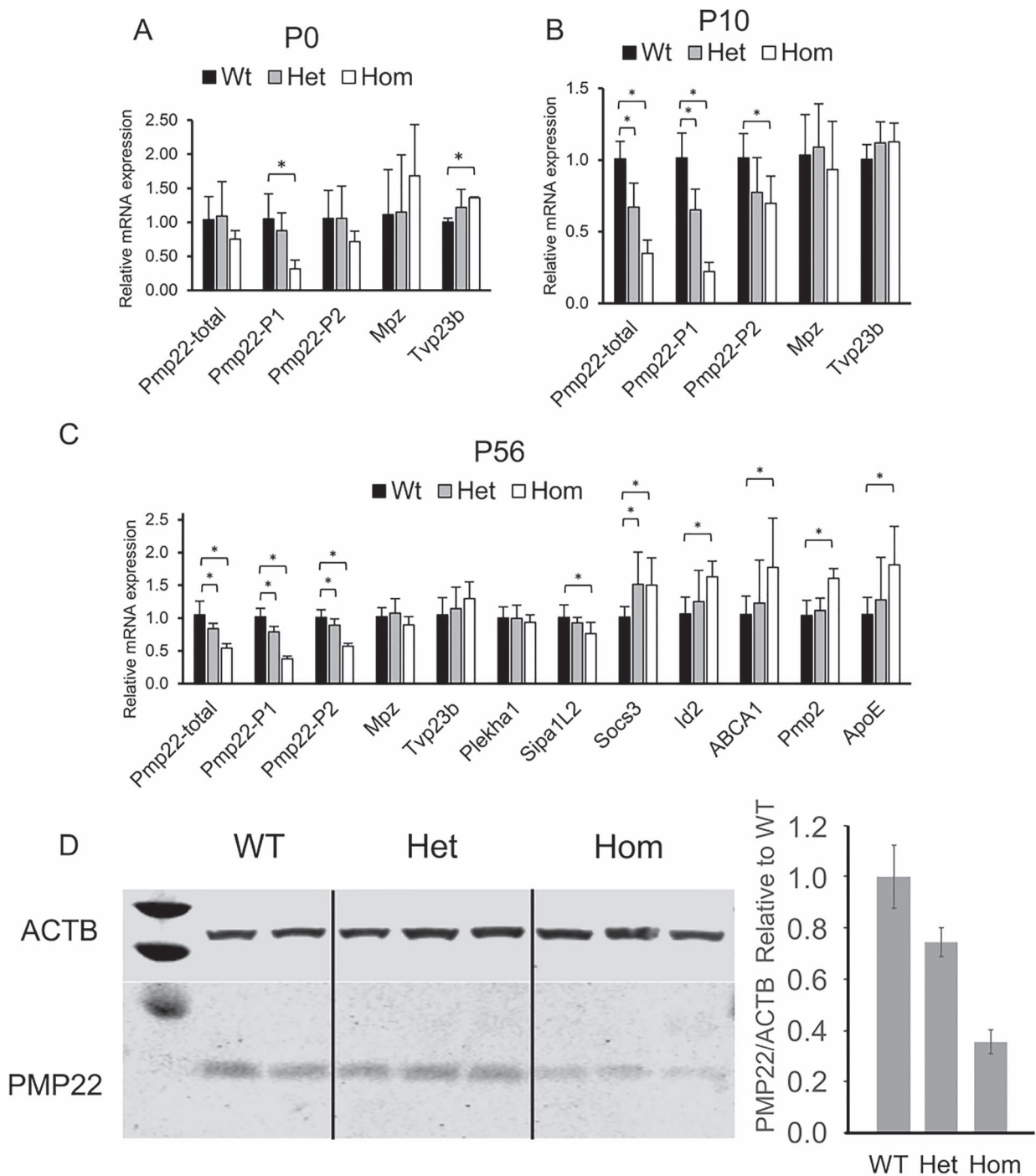


Figure 2. *Pmp22*-SE contributes to peripheral nerve *Pmp22* transcription throughout development. Expression analysis indicates the relative expression of noted genes in heterozygous and homozygous *Pmp22*-SE deletion mice relative to wild-type littermates at (A) P0 (Wt/Het/Hom $n = 3/6/4$), (B) P10 (Wt/Het/Hom $n = 5/5/3$) and (C) P56 (Wt/Het/Hom $n = 9/7/4$). Relative expression levels in P56 sciatic nerve are shown for the indicated genes. Error bars represent the standard deviation. Statistical analysis denotes results for the comparison of values in heterozygous or homozygous deletion animals to wild-type littermates ($*P < 0.05$) or comparison of homozygous to heterozygous littermates ($^{\$}P < 0.05$). (D) The western blot shows levels of PMP22 protein along with β -actin as a normalization control in the indicated genotypes. The quantitation of normalized bands relative to wild type is shown in the bar graph.

Morphometric analysis demonstrates axon loss in *Pmp22*-SE^{+/-} and *Pmp22*-SE^{-/-} nerve

Axon loss has been observed in humans with HNPP and *Pmp22*^{+/-} mice during aging (13, 14, 53), even though the axon

loss was subtle or not significant in some *Pmp22*^{+/-} mice prior to 6 months of age (33). We therefore performed morphometric analysis in *Pmp22*-SE^{+/-} and *Pmp22*-SE^{-/-} mice (Fig. 4A, 4–6 month old; $n = 5$ for each genotypic group). Again, results confirmed a mild, but statistically significant decrease of axon

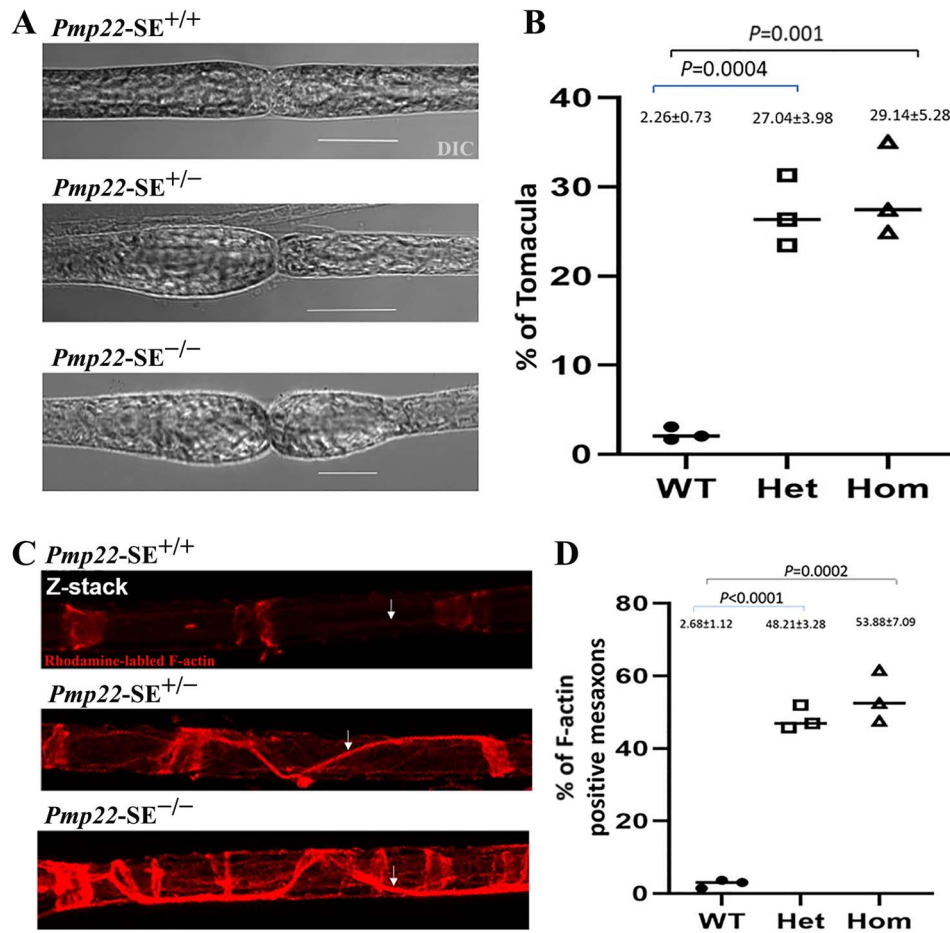


Figure 3. Increased tomacula formation and actin polymerization in *Pmp22-SE* deletion mouse sciatic nerve. (A) Images depicting tomacula formation in teased nerves of 3- to 5-month-old wild-type, *Pmp22-SE*^{+/-} and *Pmp22-SE*^{-/-} nerve. (B) The quantitation of prevalence of tomacula as the percentage of counted nerve fibers (150–300 fibers per mouse, $n=3$ mice per genotypic group). (C) Teased nerve fibers of mouse sciatic nerve were stained with fluorescent phalloidin. Arrows indicate increases in Rhodamine-labeled F-actin polymerization at and mesaxons. (D) Quantification of the prevalence of F-actin-positive mesaxons in 3- to 5-month-old wild-type, *Pmp22-SE*^{+/-} and *Pmp22-SE*^{-/-} nerve. Scale bars = 20 μ m.

density in *Pmp22-SE*^{+/-}, compared with that in wild-type nerves. As expected, the axon loss was more severe in *Pmp22-SE*^{-/-} nerves, (Table 2). This axon loss predominantly affected the small and intermediate myelinated nerve fibers, whereas larger nerve fibers were increased because of tomacula (Fig. 4B). The increase was in line with the analysis of g-ratio (axon diameter divided by outer diameter of the myelinated nerve fiber, which reflects myelin thickness). It showed a significant decrease of g-ratio in larger diameter nerve fibers (Table 2 and Fig. 4C).

Impaired recovery from conduction block in *Pmp22-SE*^{+/-} and *Pmp22-SE*^{-/-} nerve

The heterozygous deletion of *Pmp22* renders nerve susceptible to conduction block induced by mechanical compression (30). We therefore employed a model of mechanically induced nerve compression to establish whether this phenotype is present at different levels of reduced *Pmp22* expression resulting from heterozygous or homozygous deletion of *Pmp22-SE*. This was carried out by applying a precalibrated vessel clamp to compress the surgically exposed mouse sciatic nerve. Electrical stimuli were delivered to the nerve both distal and proximal to the compression site. Over time, the amplitude of nerve responses by proximal stimulation gradually declined. The latency for the decline

to reach 60% of amplitude by the distal stimulation was used as a marker to compare the nerve susceptibility to mechanical compression between wild-type and mutant mice. Consistent with prior work (30), we observed significantly shorter latency in achieving 60% conduction block in mechanically compressed nerves from both *Pmp22-SE*^{+/-} and *Pmp22-SE*^{-/-} mice compared with that in wild-type mice (Fig. 5A).

To evaluate the ability of these mice to recover from conduction block, we measured compound muscle action potential (CMAP) amplitude and nerve conduction velocity at Days 1, 3, 7 and 14 following mechanical nerve compression. In this method, surgically exposed sciatic nerve was compressed, and CMAP amplitudes were measured using both proximal stimulation (i.e. requiring transmission across compression site) and distal stimulation (i.e. with stimulus and recording being on the same side relative to the compressed point). Interestingly, despite *Pmp22-SE*^{+/-} and *Pmp22-SE*^{-/-} mice showing similar pathological changes, we observed significant differences in recovery from conduction block only in *Pmp22-SE*^{-/-} mice. In wild-type and *Pmp22-SE*^{+/-} mice, proximal CMAP amplitudes declined relative to distal stimulation at Days 1 and 3 before recovering to baseline levels by Day 14, and no significant differences were apparent between these two groups (Fig. 5B). In contrast, *Pmp22-SE*^{-/-} mice displayed much lower baseline CMAP amplitude.

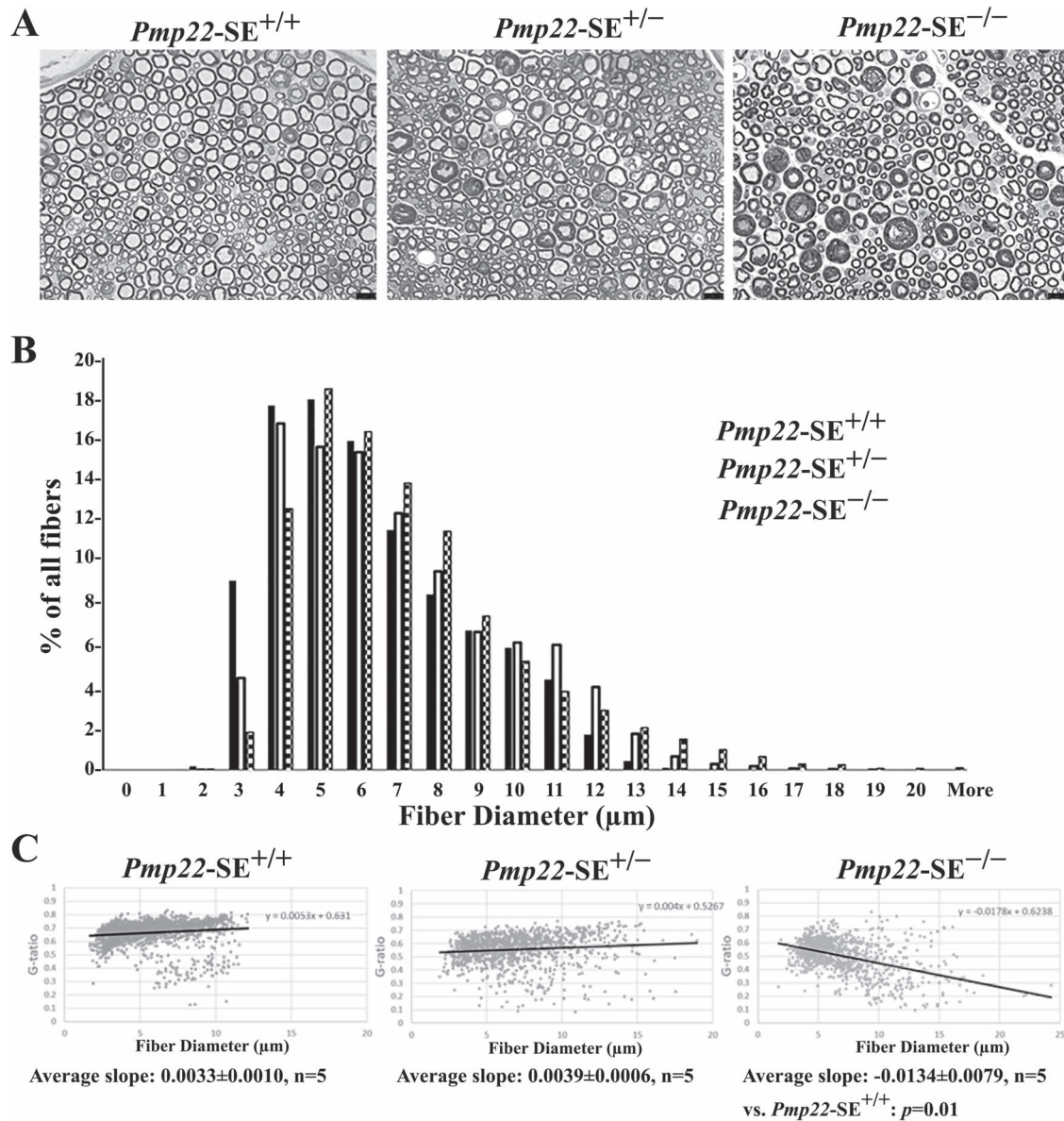


Figure 4. Morphometric analysis demonstrates axonal loss in *Pmp22-SE* deletion mouse sciatic nerve. (A) Images of the semithin section were taken from 3- to 5-month-old wild-type, *Pmp22-SE*^{+/+} and *Pmp22-SE*^{-/-} nerve. (B) Axon-diameter distributions in 3- to 5-month-old wild-type, *Pmp22-SE*^{+/-} and *Pmp22-SE*^{-/-} nerve. (C) g-Ratios were plot against axon diameters. The slope of the scatter plot reflects myelin thickness.

Although CMAP amplitude in these mice similarly decline from baseline to Day 3, there was no recovery as of Day 14 (Fig. 5B). The changes were quantitated using the proximal/distal CMAP amplitude ratio, which helps to control for differences in probe placement across multiple recording sessions. We observed significantly reduced P/D ratio only in *Pmp22-SE*^{-/-} until Day 7 after nerve compression (Fig. 5C). Similarly, although wild-type and *Pmp22-SE*^{+/-} mice displayed no significant changes in conduction velocity over this period, mice possessing homozygous deletion of *Pmp22-SE* displayed reduced conduction velocity at Days 1 and 3 after compression, with recovery to baseline levels by Day 7 (Fig. 5D).

Discussion

In this study, we describe a new mouse model of reduced *Pmp22* expression that recapitulates phenotypic and pathological

hallmarks of HNPP observed in previous rodent models of heterozygous *Pmp22* loss (12, 13, 31). We have demonstrated that a distal super-enhancer domain previously shown to regulate *Pmp22* expression *in vitro* is similarly required for full endogenous expression *in vivo*. We find that the super-enhancer contributes to gene expression at all time points evaluated and appears to selectively regulate *Pmp22* expression without affecting the nearby *Tvp23b* gene. As in our cell culture model (27), transcription from the Schwann cell-specific P1 promoter is more significantly affected by the loss of this super-enhancer throughout development. The histone H3K27 acetylation that marks the super-enhancer in peripheral nerve is absent in the central nervous system (21, 54), and this super-enhancer is required for the high expression of the Schwann cell-specific P1 promoter. However, super-enhancer deletion did not reduce total *Pmp22* mRNA levels to <30% at any age, indicating that other regulatory elements, such as the intronic regulatory element

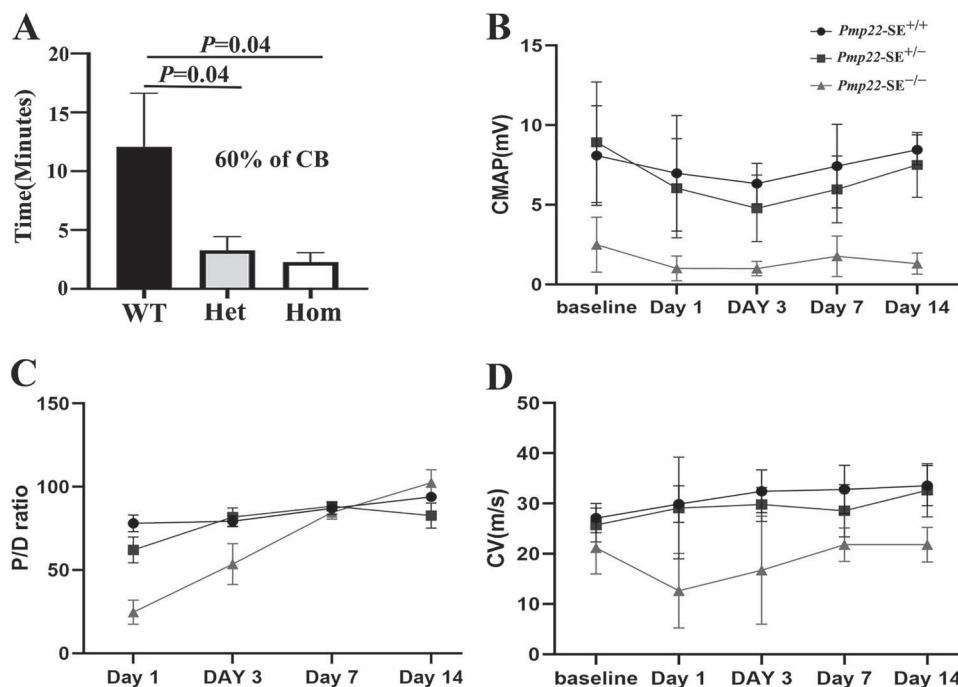


Figure 5. Impaired recovery from conduction block in *Pmp22-SE*^{-/-} mouse sciatic nerve. (A) Time to achieve 60% conduction block in 3- to 5-month-old wild-type, *Pmp22-SE*^{+/-} and *Pmp22-SE*^{-/-} nerves ($P < 0.05$; $n = 12$ mice per genotypic group). (B) CMAP amplitudes before nerve compression (baseline) and at 1, 3, 7 and 14 days following the compression. Two-way ANOVA with repeated measures showed a significant effect of genotype ($F_{2,30} = 60.96$, $P < 0.0001$) in CMAP amplitudes at all time points ($F_{3,177,95.30} = 7.665$, $P < 0.0001$), but not for CMAP recovery ($F_{8,120} = 1.309$, $P > 0.05$). Tukey's multiple comparisons showed significantly smaller CMAPs at all time points between *Pmp22-SE*^{-/-} and wild-type mice ($P < 0.0001$), but not different between *Pmp22-SE*^{+/-} and wild-type mice ($P > 0.05$). (C) Proximal/distal CMAP amplitude ratio (a measure of conduction block). The two-way ANOVA showed a significant effect of genotype ($F_{2,30} = 8.402$, $P < 0.01$) and recovery ($F_{6,90} = 6.170$, $P < 0.0001$) in P/D ratio. This difference in Day 1 was significant between *Pmp22-SE*^{-/-} and wild-type ($P < 0.0001$) or between *Pmp22-SE*^{-/-} and *Pmp22-SE*^{+/-} mice ($P < 0.01$), but not significant for the remaining time points ($P > 0.05$). (D) Nerve conduction velocity. The ANOVA showed a significant effect of genotype ($F_{2,30} = 82.01$, $P < 0.0001$), over time ($F_{2,704,81.13} = 4.958$, $P < 0.01$) and recovery ($F_{8,120} = 2.509$, $P < 0.05$). Tukey's multiple comparisons showed significantly decreased CVs at all recovery time points in *Pmp22-SE*^{-/-} animals in contrast to wild-type ($P < 0.01$) but not between wild-type and *Pmp22-SE*^{+/-} animals at any time point ($P > 0.05$).

and promoter proximal regions (20–22, 46), are also involved in maintaining proper levels of *Pmp22* expression.

Previous work evaluating 'functional demyelination' in *Pmp22*^{+/-} models has developed a model in which reduction of PMP22 protein disrupts the formation of junction protein complexes and produces hyper-permeable myelin, leading to lost internodal current and conduction block (31, 33). Here, we demonstrate a *Pmp22*-dosage-dependent progression of this mechanism, including *Pmp22*-dosage-dependent axon loss. Although both *Pmp22-SE*^{+/-} and *Pmp22-SE*^{-/-} mice also displayed tomacula and abnormal F-actin assembly, the functional consequences of conduction block and its recovery were only visible in nerves from *Pmp22-SE*^{-/-} mice. Together, these findings suggest that severity of the neuropathy is a function of the level of *Pmp22* expression.

Several different agents have been developed that can reduce PMP22 expression and improve the CMT1A neuropathy in rodent models (16, 50, 55, 56), some of which have entered clinical trials (57, 58). It has been appreciated that there is a potential risk in the development of therapeutics for CMT1A if an overly efficacious treatment reduces a patient's level of *Pmp22* expression below normal levels in healthy individuals (59). However, it remains to be determined whether development of HNPP symptoms requires reduced PMP22 levels during early myelin formation or whether a switch to reduced expression later in life is sufficient to induce the disease. In addition, a novel skin biopsy assay has been developed that can be used to evaluate levels of PMP22 expression as a target engagement assay in clinical trials (60).

In summary, we have found that a super-enhancer domain previously identified in a cultured rat Schwann cell line is an important regulator of *Pmp22* expression *in vivo*. Our data show that the loss of this super-enhancer is sufficient to induce the morphological and electrophysiological phenotype commonly associated with HNPP, which is also *Pmp22*-dosage dependent. This evidence indirectly supports the notion that previously observed upstream duplications, inclusive of the super-enhancer but not the PMP22 gene itself (23, 24), can induce a mild form of neuropathy by promoting overexpression of PMP22. More importantly, the mouse model offers a new tool to scale the levels of PMP22 *in vivo* and examines how dosages of PMP22 affect different aspects of pathogenic mechanisms in HNPP.

Materials and Methods

Experimental animals

All procedures described here were conducted in compliance with the Institutional Animal Care and Use Committees at University of Wisconsin and Wayne State University. C57BL/6 embryos and CRISPR/Cas9 reagents were electroporated at the University of Wisconsin-Madison Biotechnology Center. Guide RNA sequences are as follows: 5'-GAGGCTCAGCAAGGTCACGGGG-3' for upstream target; 5'-GCTGCTGAGGGCAGATTCGGGG-3' for downstream target. Mice from implanted embryos were genotyped to detect successful

Table 1. qPCR primers used

Gene	Forward	Reverse
<i>Actb</i>	GGGATGTTTGCTCCAACCAA	GGCGCTTTTGACTCAGGATTTA
<i>Cnp</i>	GCACCATCATCTGAGGGTTCA	TGGAAGGCATGTTGCTGTGT
<i>Gldn</i>	CCTCCACCTCCCACATTATTT	CAGAGTCTGAGGTGTCTCTTTC
<i>Pmp22pan</i>	GGCAATGGACACACGACTGA	GCTCCCAAGCGCGATGT
<i>Pmp22-P1</i>	TTGACTGCAGAGACATCCAAGTG	GGGCTCGGGATCAGAGGA
<i>Pmp22-P2</i>	AGATAGCTGTCCCTTTGAAGTAAAA	GTTGGGCTCGGGATCAGA
<i>Mag</i>	GTCCGGCACCATACTAAGTGA	TGGTTCCCCCGGAAGTG
<i>Mpz</i>	CCCTGGCCATTGTGGTTTAC	CCATTACTGGACCAGAAGGAG
<i>Tvp23b</i>	TGGCTACGTCGTATCTTGGGA	GAATCGTGTCCATTGCTCCC
<i>Pak1</i>	AACCGCTGTCTTGAGATGGA	GCAGCAATCAGTGGAGTCAG
<i>Plekha1</i>	TAGCCCTGAAGAGATGCACA	GGACGGACAGTGAATTTGGG
<i>Sipa1L2</i>	GGAACCTGAAGTGACGGAATG	ATCTTTGGATAGGACATGCTGAG
<i>Socs3</i>	GGAGATTCGCTTCGGGACT	GGAAACTTGCTGTGGGTGAC
<i>Id2</i>	ACCACCTGAAGACGGACAT	GAATTCAGACGCTGCAAGG
<i>Abca1</i>	CAACAACTCTGCCACGTGA	GCTCACTGAACCTTTGCCCA
<i>ApoE</i>	CAGTGGCCAGGAGAATCAAT	ATGTTGTTGCAGGACAGGAGAA
<i>Pmp2</i>	TGCTGGATGGGAGAATGGTAG	TGCAGACCACACCTTCATTAT

deletion using primers flanking the excised sequence: 5'-ACACACACACACATGCCAGTAAATAG-3' and 5'-TTCTCCGTGAC-TTCTGCCTCCTCATTC-3'. A single founder was identified, and F1 and F2 generation mice were backcrossed to C57/BL6 mice to generate heterozygote breeding pairs, which produced wild-type mice along with heterozygous and homozygous deletion of the *Pmp22* super-enhancer.

Genotyping

Genomic DNA was isolated from tail snips using the DNeasy Blood and Tissue kit (Qiagen). Genotyping assay was performed using GoTaq master mix (Promega) with the shared primer 5'-CATTGTTGGGATGTGCTCTTAGTCT-3' and genotype-specific reverse primers: 5'-CAAGAGAAGGTTAAAGCTATGCCA-3' (for detection of deletion postrepair junction) and 5'-CATTGAGTGAAGGAGAACAACGG-3' (for amplification of wild-type sequence). Sex determination of P0 mice was performed via PCR with the following primers: 5'-TGCAGTCTACTCCAGTCTTG-3' and 5'-GATCTTGATTTTAGTGTTC-3' to amplify a portion of the *Sry* gene on the Y chromosome.

Reverse transcription-quantitative polymerase chain reaction

RNA was isolated from sciatic nerves using TRIzol reagent (Ambion) and the RNEasy MinElute cleanup kit (Qiagen) according to the manufacturer's protocol. RNA was converted to complementary DNA using MMLV reverse transcriptase (Invitrogen). Reverse transcription-quantitative polymerase chain reaction (RT-qPCR) experiments were performed using Power SYBR Green master mix (Thermo Fisher Scientific) on the StepOne Plus and/or ViiA7 systems (Applied Biosystems). Relative expression was calculated using the comparative Ct method (61). Primers are listed in Table 1.

Nerve compression and nerve conduction studies

Nerve conduction studies were performed as described previously (30, 33). Sciatic nerve was surgically exposed and

compressed with a precalibrated vessel clamp (cat#: TKF-1-15g, AROS Surgical Instruments Co.). CMAP was recorded with both proximal and distal stimulation, and the proximal/distal (P/D) CMAP amplitude ratio was calculated to define the degrees of conduction block and minimize effects of variation in electrode placement for multiple trials with the same animal.

Semithin section

As described (62), tissues were fixed with 4% paraformaldehyde. Nerves were embedded in Epon and sectioned to semithin sections for morphometric analysis.

Teased nerve fiber imaging and immunofluorescence

As described (31, 33), nerves were fixed in 4% paraformaldehyde and teased into individual nerve fibers on glass slides. Immunostaining with antibodies against myelin proteins was visualized under confocal microscopy. Tomacula were counted under light microscopy. For F-actin staining, teased fibers were stained with rhodamine-conjugated phalloidin and imaged with a fluorescent microscope.

Morphometric analysis

Morphometric analysis was performed as described previously (63). All $\times 63$ bright field images of mouse sciatic nerves were taken using a Leica microscope. A trained deep learning model was applied to the images to generate semantic segmentations with isolated myelin or axon. Each nerve fiber's inner area around the axon and outer areas (axon + myelin) were measured. Then, each fiber's diameter, myelin thickness and g-ratio were calculated. Myelinated fiber density, myelin thickness and g-ratio were analyzed using paired two-tailed t-tests ($n=5$ for each of the 3 genotypes) (Table 2). A histogram with 1 μm bin size reflecting a proportion of fibers of certain diameter was generated for each genotype to better visualize axon loss of specific fiber diameters in the mutant nerves.

Table 2. Axon density and g-ratio in *Pmp22*-SE deletion sciatic nerve

	<i>Pmp22</i> -SE ^{+/+}	<i>Pmp22</i> -SE ^{+/-}	<i>Pmp22</i> -SE ^{-/-}
Mouse number	5	5	5
Fiber number	8503	7243	5196
Axon density	19939 ± 1328	16904 ± 1556	12958 ± 1394
P-value		0.018 ^a	0.000 ^a ; 0.006 ^b
g-Ratio	0.67 ± 0.01	0.61 ± 0.03	0.54 ± 0.04
P-value		0.021 ^a	0.004 ^a ; 0.038 ^b

^a*Pmp22*-SE^{+/-} or *Pmp22*-SE^{-/-} versus *Pmp22*-SE^{+/+}.^b*Pmp22*-SE^{-/-} versus *Pmp22*-SE^{+/-}.

Western blot

To prepare western blot lysates, a single nerve from each study animal was briefly thawed on ice then disrupted with a micro-centrifuge pestle in 200 µl of ×1 Laemmli buffer containing 5% β-mercaptoethanol v/v, protease (Sigma P8340) and phosphatase inhibitors. Following tissue lysis, samples were heated at 95°C for 5 min and then centrifuged at 15 000g for 15 min. Supernatants were run on a 12% TEO-Tricine SDS gel (Expedeon BCG01212) and transferred to nitrocellulose membrane (Amersham Protran 10600015). Membrane was blocked with 5% non-fat dry milk, then incubated overnight at 4°C with primary antibodies: Mouse anti-ACTB (AbClonal AC004) 1:5000 and Rabbit anti-PMP22 (LsBio LS-C383645) 1:250. Membrane was washed 3 times with Tris-buffered saline with Tween 20 (TBST), then incubated for 1 h at room temperature with secondary antibodies: Gt anti-Mouse IR 800CW (Licor 925-32210) 1:10 000 and Donkey anti-Rabbit IR 800CW (Licor 925-32213) 1:10 000. Blot was imaged using the Odyssey imaging system, and PMP22 bands were normalized to ACTB.

Statistical analysis

The data are represented as the mean ± SD. Statistical analysis was performed using SPSS software. P-values were obtained from the Student's two-tailed t-test or repeated measures analysis of variance ($P < 0.05$ is considered to be statistically significant).

Acknowledgements

We wish to thank members of our laboratories for feedback on this study.

Funding

The National Institutes of Health (RO1 NS083841 to J.S., RO1 NS066927 and RO1 NS115748 to J.L. and U54 core grant HD090256).

Conflict of Interest: None declared.

References

- Pereira, J.A., Lebrun-Julien, F. and Suter, U. (2012) Molecular mechanisms regulating myelination in the peripheral nervous system. *Trends Neurosci.*, **35**, 123–134.
- Lupski, J.R., de Oca-Luna, R.M., Slaugenhaupt, S., Pentao, L., Guzzetta, V., Trask, B.J., Saucedo-Cardenas, O., Barker, D.F., Killian, J.M., Garcia, C.A. et al. (1991) DNA duplication associated with Charcot-Marie-Tooth disease type 1A. *Cell*, **66**, 219–232.

- Raeymaekers, P., Timmerman, V., Nelis, E., De Jonghe, P., Hoogendijk, J.E., Baas, F., Barker, D.F., Martin, J.J., De Visser, M. and Bolhuis, P.A. (1991) Duplication in chromosome 17p11.2 in Charcot-Marie-Tooth neuropathy type 1a (CMT 1a). The HMSN Collaborative Research Group. *Neuromuscul. Disord.*, **1**, 93–97.
- Snipes, G.J., Suter, U., Welcher, A.A. and Shooter, E.M. (1992) Characterization of a novel peripheral nervous system myelin protein (PMP-22/SR13). *J. Cell Biol.*, **117**, 225–238.
- Patel, P.I., Roa, B.B., Welcher, A.A., Schoener-Scott, R., Trask, B.J., Pentao, L., Snipes, G.J., Garcia, C.A., Francke, U., Shooter, E.M. et al. (1992) The gene for the peripheral myelin protein PMP-22 is a candidate for Charcot-Marie-Tooth disease type 1A. *Nat. Genet.*, **1**, 159–165.
- Saporta, M.A., Katona, I., Lewis, R.A., Masse, S., Shy, M.E. and Li, J. (2009) Shortened internodal length of dermal myelinated nerve fibres in Charcot-Marie-Tooth disease type 1A. *Brain*, **132**, 3263–3273.
- Gabreëls-Festen, A. and Wetering, R.V. (1999) Human nerve pathology caused by different mutational mechanisms of the PMP22 gene. *Ann. N. Y. Acad. Sci.*, **883**, 336–343.
- Gabreëls-Festen, A.A., Bolhuis, P.A., Hoogendijk, J.E., Valentijn, L.J., Eshuis, E.J. and Gabreëls, F.J. (1995) Charcot-Marie-Tooth disease type 1A: morphological phenotype of the 17p duplication versus PMP22 point mutations. *Acta Neuropathol.*, **90**, 645–649.
- Li, J., Bai, Y., Ghandour, K., Qin, P., Grandis, M., Trostinskaia, A., Ianakova, E., Wu, X., Schenone, A., Vallat, J.M. et al. (2005) Skin biopsies in myelin-related neuropathies: bringing molecular pathology to the bedside. *Brain*, **128**, 1168–1177.
- Chance, P.F., Alderson, M.K., Leppig, K.A., Lensch, M.W., Matsumami, N., Smith, B., Swanson, P.D., Odelberg, S.J., Disteche, C.M. and Bird, T.D. (1993) DNA deletion associated with hereditary neuropathy with liability to pressure palsies. *Cell*, **72**, 143–151.
- Nicholson, G.A., Valentijn, L.J., Cherryson, A.K., Kennerson, M.L., Bragg, T.L., DeKroon, R.M., Ross, D.A., Pollard, J.D., McLeod, J.G. and Bolhuis, P.A. (1994) A frame shift mutation in the PMP22 gene in hereditary neuropathy with liability to pressure palsies. *Nat. Genet.*, **6**, 263–266.
- Adlkofer, K., Martini, R., Aguzzi, A., Zielasek, J., Toyka, K.V. and Suter, U. (1995) Hypermyelination and demyelinating peripheral neuropathy in *Pmp22*-deficient mice. *Nat. Genet.*, **11**, 274–280.
- Adlkofer, K., Frei, R., Neuberger, D.H., Zielasek, J., Toyka, K.V. and Suter, U. (1997) Heterozygous peripheral myelin protein 22-deficient mice are affected by a progressive demyelinating tomaculous neuropathy. *J. Neurosci.*, **17**, 4662–4671.
- Li, J., Ghandour, K., Radovanovic, D., Shy, R.R., Krajewski, K.M., Shy, M.E. and Nicholson, G.A. (2007) Stoichiometric

- alteration of PMP22 protein determines the phenotype of hereditary neuropathy with liability to pressure palsies. *Arch. Neurol.*, **64**, 974–978.
15. Horowitz, S.H., Spollen, L.E. and Yu, W. (2004) Hereditary neuropathy with liability to pressure palsy: fulminant development with axonal loss during military training. *J. Neurol. Neurosurg. Psychiatry*, **75**, 1629–1631.
 16. Pantera, H., Shy, M.E. and Svaren, J. (1726) Regulating PMP22 expression as a dosage sensitive neuropathy gene. *Brain Res.*, **2020**, 146491.
 17. Ma, K.H., Duong, P., Moran, J.J., Junaidi, N. and Svaren, J. (2018) Polycomb repression regulates Schwann cell proliferation and axon regeneration after nerve injury. *Glia*, **66**, 2487–2502.
 18. Suter, U., Snipes, G.J., Schoener-Scott, R., Welcher, A.A., Pareek, S., Lupski, J.R., Murphy, R.A., Shooter, E.M. and Patel, P.I. (1994) Regulation of tissue-specific expression of alternative peripheral myelin protein-22 (PMP22) gene transcripts by two promoters. *J. Biol. Chem.*, **269**, 25795–25808.
 19. Maier, M., Berger, P., Nave, K.A. and Suter, U. (2002) Identification of the regulatory region of the peripheral myelin protein 22 (PMP22) gene that directs temporal and spatial expression in development and regeneration of peripheral nerves. *Mol. Cell. Neurosci.*, **20**, 93–109.
 20. Maier, M., Castagner, F., Berger, P. and Suter, U. (2003) Distinct elements of the peripheral myelin protein 22 (PMP22) promoter regulate expression in Schwann cells and sensory neurons. *Mol. Cell. Neurosci.*, **24**, 803–817.
 21. Lopez-Anido, C., Poitelon, Y., Gopinath, C., Moran, J.J., Ma, K.H., Law, W.D., Antonellis, A., Feltri, M.L. and Svaren, J. (2016) Tead1 regulates the expression of peripheral myelin protein 22 during Schwann cell development. *Hum. Mol. Genet.*, **25**, 3055–3069.
 22. Jones, E.A., Brewer, M.H., Srinivasan, R., Krueger, C., Sun, G., Charney, K.N., Keles, S., Antonellis, A. and Svaren, J. (2012) Distal enhancers upstream of the Charcot-Marie-Tooth type 1A disease gene PMP22. *Hum. Mol. Genet.*, **21**, 1581–1591.
 23. Weterman, M.A., van Ruissen, F., de Wissel, M., Bordewijk, L., Samijn, J.P., van der Pol, W.L., Meggouh, F. and Baas, F. (2010) Copy number variation upstream of PMP22 in Charcot-Marie-Tooth disease. *Eur. J. Hum. Genet.*, **18**, 421–428.
 24. Zhang, F., Seeman, P., Liu, P., Weterman, M.A., Gonzaga-Jauregui, C., Towne, C.F., Batish, S.D., De Vriendt, E., De Jonghe, P., Rautenstrauss, B. et al. (2010) Mechanisms for non-recurrent genomic rearrangements associated with CMT1A or HNPP: rare CNVs as a cause for missing heritability. *Am. J. Hum. Genet.*, **86**, 892–903.
 25. Hung, H.A., Sun, G., Keles, S. and Svaren, J. (2015) Dynamic regulation of Schwann cell enhancers after peripheral nerve injury. *J. Biol. Chem.*, **290**, 6937–6950.
 26. Welcher, A.A., Suter, U., De Leon, M., Snipes, G.J. and Shooter, E.M. (1991) A myelin protein is encoded by the homologue of a growth arrest-specific gene. *Proc. Natl. Acad. Sci. U. S. A.*, **88**, 7195–7199.
 27. Pantera, H., Moran, J.J., Hung, H.A., Pak, E., Dutra, A. and Svaren, J. (2018) Regulation of the neuropathy-associated Pmp22 gene by a distal super-enhancer. *Hum. Mol. Genet.*, **27**, 2830–2839.
 28. Amici, S.A., Dunn, W.A., Murphy, A.J., Adams, N.C., Gale, N.W., Valenzuela, D.M., Yancopoulos, G.D. and Notterpek, L. (2006) Peripheral myelin protein 22 is in complex with alpha6beta4 integrin, and its absence alters the Schwann cell basal lamina. *J. Neurosci.*, **26**, 1179–1189.
 29. Amici, S.A., Dunn, W.A. and Notterpek, L. (2007) Developmental abnormalities in the nerves of peripheral myelin protein 22-deficient mice. *J. Neurosci. Res.*, **85**, 238–249.
 30. Bai, Y., Zhang, X., Katona, I., Saporta, M.A., Shy, M.E., O'Malley, H.A., Isom, L.L., Suter, U. and Li, J. (2010) Conduction block in PMP22 deficiency. *J. Neurosci.*, **30**, 600–608.
 31. Guo, J., Wang, L., Zhang, Y., Wu, J., Arpag, S., Hu, B., Imhof, B.A., Tian, X., Carter, B.D., Suter, U. et al. (2014) Abnormal junctions and permeability of myelin in PMP22-deficient nerves. *Ann. Neurol.*, **75**, 255–265.
 32. Rosso, G., Liashkovich, I., Gess, B., Young, P., Kun, A. and Shahin, V. (2014) Unravelling crucial biomechanical resilience of myelinated peripheral nerve fibres provided by the Schwann cell basal lamina and PMP22. *Sci. Rep.*, **4**, 7286.
 33. Hu, B., Arpag, S., Zhang, X., Möbius, W., Werner, H., Sosinsky, G., Ellisman, M., Zhang, Y., Hamilton, A., Chernoff, J. et al. (2016) Tuning PAK activity to rescue abnormal myelin permeability in HNPP. *PLoS Genet.*, **12**, e1006290.
 34. Poitelon, Y., Matafora, V., Silvestri, N., Zambroni, D., McGarry, C., Serghany, N., Rush, T., Vizzuso, D., Court, F.A., Bachi, A. et al. (2018) A dual role for integrin $\alpha 6 \beta 4$ in modulating hereditary neuropathy with liability to pressure palsies. *J. Neurochem.*, **145**, 245–257.
 35. Zhou, Y., Miles, J.R., Tavori, H., Lin, M., Khoshbouei, H., Borchelt, D.R., Bazick, H., Landreth, G.E., Lee, S., Fazio, S. et al. (2019) PMP22 regulates cholesterol trafficking and ABCA1-mediated cholesterol efflux. *J. Neurosci.*, **39**, 5404–5418.
 36. Feltri, M.L., Scherer, S.S., Nemni, R., Kamholz, J., Vogelbacker, H., Scott, M.O., Canal, N., Quaranta, V. and Wrabetz, L. (1994) Beta 4 integrin expression in myelinating Schwann cells is polarized, developmentally regulated and axonally dependent. *Development*, **120**, 1287–1301.
 37. Nodari, A., Previtali, S.C., Dati, G., Occhi, S., Court, F.A., Colombelli, C., Zambroni, D., Dina, G., Del Carro, U., Campbell, K.P. et al. (2008) Alpha6beta4 integrin and dystroglycan cooperate to stabilize the myelin sheath. *J. Neurosci.*, **28**, 6714–6719.
 38. Srinivasan, R., Sun, G., Keles, S., Jones, E.A., Jang, S.W., Krueger, C., Moran, J.J. and Svaren, J. (2012) Genome-wide analysis of EGR2/SOX10 binding in myelinating peripheral nerve. *Nucleic Acids Res.*, **40**, 6449–6460.
 39. Lopez-Anido, C., Sun, G., Koenning, M., Srinivasan, R., Hung, H.A., Emery, B., Keles, S. and Svaren, J. (2015) Differential SOX10 genomic occupancy in myelinating glia. *Glia*, **63**, 1897–1914.
 40. Deng, Y., Wu, L.M.N., Bai, S., Zhao, C., Wang, H., Wang, J., Xu, L., Sakabe, M., Zhou, W., Xin, M. et al. (2017) A reciprocal regulatory loop between TAZ/YAP and G-protein $G_{\alpha s}$ regulates Schwann cell proliferation and myelination. *Nat. Commun.*, **8**, 15161.
 41. Ma, K.H., Hung, H.A. and Svaren, J. (2016) Epigenomic regulation of Schwann cell reprogramming in peripheral nerve injury. *J. Neurosci.*, **36**, 9135–9147.
 42. Verdier, V., Csárdi, G., de Preux-Charles, A.S., Médard, J.J., Smit, A.B., Verheijen, M.H., Bergmann, S. and Chrast, R. (2012) Aging of myelinating glial cells predominantly affects lipid metabolism and immune response pathways. *Glia*, **60**, 751–760.
 43. Svaren, J. and Meijer, D. (2008) The molecular machinery of myelin gene transcription in Schwann cells. *Glia*, **56**, 1541–1551.
 44. Jang, S.W., Srinivasan, R., Jones, E.A., Sun, G., Keles, S., Krueger, C., Chang, L.W., Nagarajan, R. and Svaren, J. (2010)

- Locus-wide identification of Egr2/Krox20 regulatory targets in myelin genes. *J. Neurochem.*, **115**, 1409–1420.
45. He, Y., Kim, J.Y., Dupree, J., Tewari, A., Melendez-Vasquez, C., Svaren, J. and Casaccia, P. (2010) Yy1 as a molecular link between neuregulin and transcriptional modulation of peripheral myelination. *Nat. Neurosci.*, **13**, 1472–1480.
 46. Jones, E.A., Lopez-Anido, C., Srinivasan, R., Krueger, C., Chang, L.W., Nagarajan, R. and Svaren, J. (2011) Regulation of the PMP22 gene through an intronic enhancer. *J. Neurosci.*, **31**, 4242–4250.
 47. LeBlanc, S.E., Srinivasan, R., Ferri, C., Mager, G.M., Gillian-Daniel, A.L., Wrabetz, L. and Svaren, J. (2005) Regulation of cholesterol/lipid biosynthetic genes by Egr2/Krox20 during peripheral nerve myelination. *J. Neurochem.*, **93**, 737–748.
 48. Zorick, T.S., Syroid, D.E., Arroyo, E., Scherer, S.S. and Lemke, G. (1996) The transcription factors SCIP and Krox-20 mark distinct stages and cell fates in Schwann cell differentiation. *Mol. Cell. Neurosci.*, **8**, 129–145.
 49. Topilko, P., Levi, G., Merlo, G., Mantero, S., Desmarquet, C., Mancardi, G. and Charnay, P. (1997) Differential regulation of the zinc finger genes Krox-20 and Krox-24 (Egr-1) suggests antagonistic roles in Schwann cells. *J. Neurosci. Res.*, **50**, 702–712.
 50. Zhao, H.T., Damle, S., Ikeda-Lee, K., Kuntz, S., Li, J., Mohan, A., Kim, A., Hung, G., Scheideler, M.A., Scherer, S.S. et al. (2018) PMP22 antisense oligonucleotides reverse Charcot-Marie-Tooth disease type 1A features in rodent models. *J. Clin. Invest.*, **128**, 359–368.
 51. Tao, F., Beecham, G.W., Rebelo, A.P., Svaren, J., Blanton, S.H., Moran, J.J., Lopez-Anido, C., Morrow, J.M., Abreu, L., Rizzo, D. et al. (2019) Variation in SIPA1L2 is correlated with phenotype modification in Charcot-Marie-Tooth disease type 1A. *Ann. Neurol.*, **85**, 316–330.
 52. Giambonini-Brugnoli, G., Buchstaller, J., Sommer, L., Suter, U. and Mantei, N. (2005) Distinct disease mechanisms in peripheral neuropathies due to altered peripheral myelin protein 22 gene dosage or a Pmp22 point mutation. *Neurobiol. Dis.*, **18**, 656–668.
 53. Sancho, S., Magyar, J.P., Aguzzi, A. and Suter, U. (1999) Distal axonopathy in peripheral nerves of PMP22-mutant mice. *Brain*, **122**, 1563–1577.
 54. Yu, Y., Chen, Y., Kim, B., Wang, H., Zhao, C., He, X., Liu, L., Liu, W., Wu, L.M., Mao, M. et al. (2013) Olig2 targets chromatin remodelers to enhancers to initiate oligodendrocyte differentiation. *Cell*, **152**, 248–261.
 55. Passage, E., Norreel, J., Noack-Fraissignes, P., Sanguedolce, V., Pizant, J., Thirion, X., Robaglia-Schlupp, A., Pellissier, J. and Fontés, M. (2004) Ascorbic acid treatment corrects the phenotype of a mouse model of Charcot-Marie-Tooth disease. *Nat. Med.*, **10**, 396–401.
 56. Prukop, T., Stenzel, J., Wernick, S., Kungl, T., Mroczek, M., Adam, J., Ewers, D., Nabirotkin, S., Nave, K.A., Hajj, R. et al. (2019) Early short-term PXT3003 combinational therapy delays disease onset in a transgenic rat model of Charcot-Marie-Tooth disease 1A (CMT1A). *PLoS One*, **14**, e0209752.
 57. Pareyson, D., Reilly, M.M., Schenone, A., Fabrizi, G.M., Cavallaro, T., Santoro, L., Vita, G., Quattrone, A., Padua, L., Gemignani, F. et al. (2011) Ascorbic acid in Charcot-Marie-Tooth disease type 1A (CMT-TRIAAL and CMT-TRAUK): a double-blind randomised trial. *Lancet Neurol.*, **10**, 320–328.
 58. Attarian, S., Vallat, J.M., Magy, L., Funalot, B., Gonnaud, P.M., Lacour, A., Péréon, Y., Dubourg, O., Pouget, J., Micallef, J. et al. (2014) An exploratory randomised double-blind and placebo-controlled phase 2 study of a combination of baclofen, naltrexone and sorbitol (PXT3003) in patients with Charcot-Marie-Tooth disease type 1A. *Orphanet J. Rare Dis.*, **9**, 199.
 59. Li, J. (2017) Caveats in the established understanding of CMT1A. *Ann. Clin. Transl. Neurol.*, **4**, 601–607.
 60. Svaren, J., Moran, J.J., Wu, X., Zuccarino, R., Bacon, C., Bai, Y., Ramesh, R., Gutmann, L., Anderson, D.M., Pavelec, D. et al. (2019) Schwann cell transcript biomarkers for hereditary neuropathy skin biopsies. *Ann. Neurol.*, **85**, 887–898.
 61. Livak, K.J. and Schmittgen, T.D. (2001) Analysis of relative gene expression data using real-time quantitative PCR and the 2^{-ΔΔC_T} method. *Methods*, **25**, 402–408.
 62. Zhang, X., Chow, C.Y., Sahenk, Z., Shy, M.E., Meisler, M.H. and Li, J. (2008) Mutation of FIG4 causes a rapidly progressive, asymmetric neuronal degeneration. *Brain*, **131**, 1990–2001.
 63. Moiseev, D., Hu, B. and Li, J. (2019) Morphometric analysis of peripheral myelinated nerve fibers through deep learning. *J. Peripher. Nerv. Syst.*, **24**, 87–93.